Metal Ions in the Circumgalactic Medium

E.O. Vasiliev[1,2], M.V. Ryabova[1], Yu.A. Shchekinov[3]

E-mail: *eugstar@mail.ru*

Recent observations show high column densities of metal ions in extended haloes of galaxies within $z \sim 0$–0.5. For instance, to explain column densities of OVI ion observed around star-forming galaxies one should assume solar metallicity in the extended haloes, and in this case the haloes become the main reservoir of missing baryons and metals. Using time-dependent radiation field of a nearby starburst galaxy we study how ionic species depend on the galactic mass and star formation rate. We derive conditions for the high ionic states of metals to appear in extended galactic haloes.

1 Introduction and model description

High column densities of OVI and CIV ions in halos of star-forming galaxies lead to a conclusion on more massive galactic halos than thought before [1, 2]. In principle, this conclusion for galactic haloes to bear such a large gas mass might solve the problem of missing baryons and metals, though requiring enormously high oxygen production and mass ejection rates. Taking into account galactic ionizing radiation, the maximum OVI fraction can reach ∼0.4–0.9 that facilitates constrains on both gaseous mass and metallicity for massive star-forming galaxies [3]. Here we are interested in metal column densities in circumgalactic medium of less massive galaxies with special attention for CIV and OVI ions. We present only a brief description of our model, the details will be presented in our future paper.

Using the photoionization code CLOUDY [4] we calculate all ionization states of the elements H, He, C, N, O, Ne, Mg, Si and Fe. In our calculations the gas in the circumgalactic medium is in local thermal equilibrium that means the equality between cooling and heating rates in a gas parcel located at the radial distance r from the galactic center and exposed to both galactic (reached to such distance) and extragalactic radiation. In order to follow evolution of stellar mass, metallicity and galaxy spectrum, we use the spectrophotometric code PEGASE [5]. We assume a Schmidt-like power-law star formation rate (SFR) typical of star-forming galaxies: $\mathrm{SFR}(t) = \mathcal{M}_g^{p_1}/p_2$, where $\mathcal{M}$ is the normalized mass of gas in $M_\odot$. In our model we assume a closed-box regime. To extend the spectrum to higher energies (up to $\sim 10^4$ eV), we use the empirical relation between the X-ray luminosity and the star formation rate [6]. For the extragalactic background we accept the

[1] Southern Federal University, Russia
[2] Special Astrophysical Observatory, Russian Academy of Sciences (RAS), Russia
[3] Astro Space Center of Lebedev Physical Institute of RAS, Russia

V. Grinin et al. (eds) Radiation mechanisms of astrophysical objects. Yerevan: Edit Print, 2017, pp. 127–132.

Table 1: List of the main models

Total mass of gas $M_g^i, M_\odot$	p_2, Myr/$M_\odot$ (Name of model)
10^{10}	3×10^5 (A1), 3×10^4 (A2), 3×10^3 (A3)
5×10^{10}	3×10^5 (B1), 3×10^4 (B2), 3×10^3 (B3)
10^{11}	3×10^5 (C1), 3×10^4 (C2), 3×10^3 (C3)

spectrum described in [7]. We suppose the density profile has a shape similar to the Milky Way galaxy [8] normalized to mass of the dark matter halo. The parameters of the models are listed in Table 1. A fiducial value of gas metallicity in our models is assumed to be equal to 0.1 $Z_\odot$.

2 Results

We consider gas in outer haloes of star-forming galaxies with stellar mass $\sim10^9 - 10^{11}$ $M_\odot$. Figure 1 shows the dependence of specific star formation rate, sSFR = SFR/M_*, on the stellar mass, M_*. Note that the value of p_2 increases from left to right. It is clearly seen that almost all points for the COS-Dwarfs galaxies are locked between tracks for models A1–C2 as well as the data for the star-forming COS-Halos galaxies are close to the tracks of the models C2–C3. Therefore, we expect that spectral properties of the galaxies observed in the COS-Dwarfs and COS-Halos surveys are similar to those in the models considered here during the latest ∼3–4 Gyrs of their evolution.

Figure 2 shows the dependence of CIV column densities (left panels) in a halo around a galaxy in models B*. The N(CIV) values become lower with a decrease of both impact distance b and HI column density in the disk. This is explained by an increase of photons ionized CIV, so that under such conditions carbon is locked mainly in CV state. High column densities, $N(\mathrm{CIV}) \gtrsim 10^{14}$ cm^{-2}, are found at impact distances $b \lesssim 0.3\,r_v$, moderate values $\sim10^{13.5}$–10^{14} cm^{-2} can be detected at larger distances $b \sim (0.3\text{–}0.5)\,r_v$. Certainly, the increase of SFR from model B1 (upper panel) to B3 (lower panel) leads to reducing N(CIV), especially this is clear for moderate values of HI column density $\sim10^{20}$–$10^{20.4}$ cm^{-2}. However, the N(CIV) values calculated for galaxies in models B* and $N(\mathrm{HI}) \gtrsim 10^{20.4}$ cm^{-2} are close to the measured ones in the COS-Dwarfs survey [2]. Note that the stellar masses and SFR in models B* are also similar to those detected for the host galaxies in the survey (Fig. 1). One can see that N(CIV) significantly depends on the absorption of galactic radiation.

Figure 2 shows the OVI column densities (right panels) in a halo around a galaxy in models B*. Similar to N(CIV) the OVI column density reaches values as high as $\sim10^{13.8}$ cm^{-2} at $b \lesssim 0.5\,r_v$, but contrary to CIV it increases for smaller absorption of the galactic radiation: N(OVI) becomes $\sim10^{14.2-15}$ cm^{-2} for $N(\mathrm{HI}) \lesssim 10^{20.3}$ cm^{-2}. Higher SFR is also favor to higher N(OVI). Such behavior is due to a growth of galactic photons being able to ionize OV.

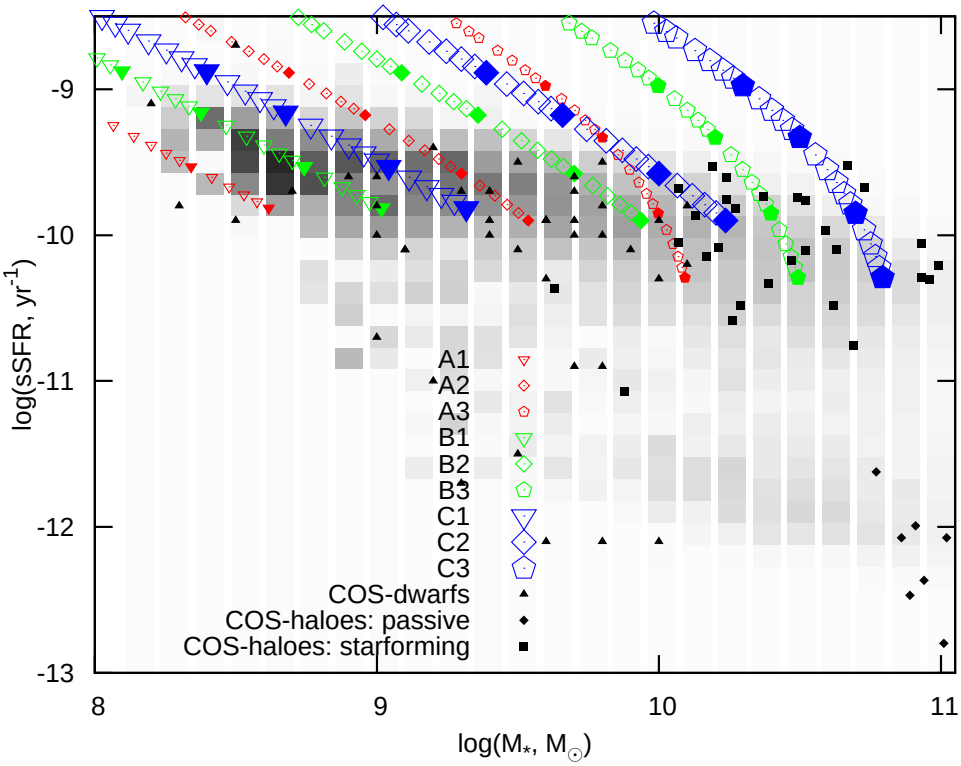

Figure 1: The dependence of specific star formation rate, sSFR = SFR/M_*, on the stellar mass, M_*, for the models A*, B* and C* showed by small, middle-size and large open symbols (Table 1). The value of p_2 increases from left to right. The filled symbols among open ones correspond to 1, 2, 5 and 10 billion years (from top-left to bottom-right points) passed from the beginning of the evolution of a galaxy. Data for the COS-Dwarfs galaxies from [2] are shown by small filled triangles and for the COS-Halos star-forming and passive galaxies from [1] are depicted by small filled squares and rhombuses, respectively. The gray-scale map is for SDSS+GALEX galaxies [9].

Note that both CIV and OVI column densities are as high as $\sim 10^{14-14.5}$ cm^{-2} and $\sim 10^{14.5-15}$ cm^{-2}, respectively, at small $b \lesssim 0.2$ for moderate values of N(HI) $\sim 10^{20.4}$ cm^{-2}. Whereas in other ranges of N(HI) and b either CIV or OVI has high column density, in other words, there takes place the bimodal distribution. It has been argued [2] that high CIV column densities can be found in halos of dwarf galaxies, whereas high OVI values are usual in a gas around massive star-forming galaxies [1], and have assumed the existence of bimodality over mass of a galaxy. Here we consider the same total and initial gaseous masses of a galaxy (in models B* the initial gaseous mass equals 5×10^5 $M_\odot$, see Table 1), but the SFR is taken different, so that during the evolution the stellar masses reach different values ranged by more than an order of magnitude (middle-size green symbols in Fig. 1). However, Figure 2 shows similar N(OVI) distributions for all three values of SFR and significant dependence of N(OVI) on HI column density.

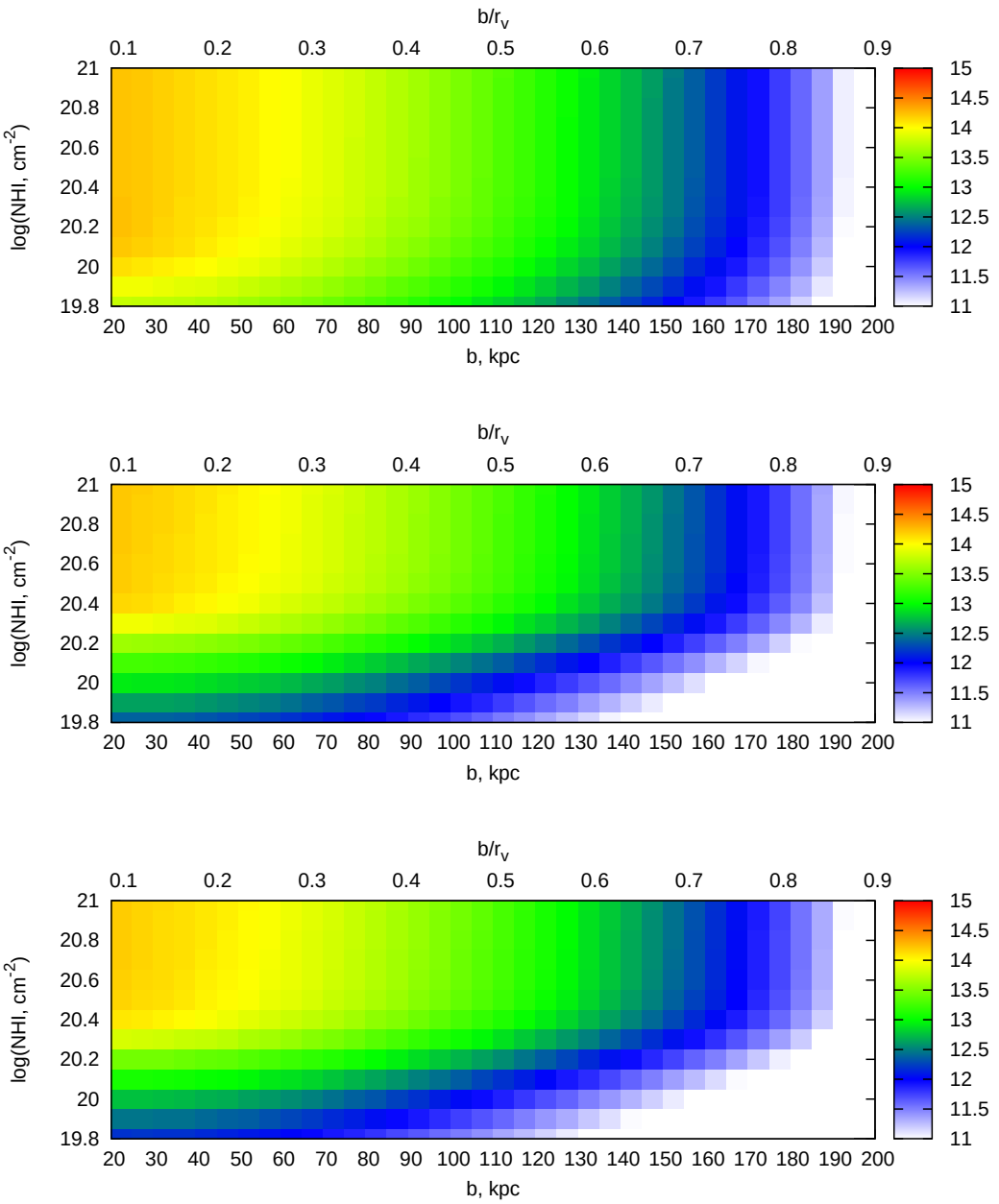

Figure 2: The dependence of CIV (*left* panels) and OVI (*right* panels) column densities (in logarithmic scale) in a halo around a galaxy in models B* on impact parameter b (which is given in kpc in the lower x-axis and in units of virial radius r_v of a galaxy in the upper x-axis) and the HI column density $\log N_{\rm HI}$ in the galactic disk. The upper row corresponds to model B1 ($M = 5 \times 10^{10}\ M_\odot$, $p_2 = 3 \times 10^5$ Myr$/M_\odot$), the middle is for model B2 ($M = 5 \times 10^{10}\ M_\odot$, $p_2 = 3 \times 10^4$ Myr$/M_\odot$), and the lower one is for B3 ($M = 5 \times 10^{10}\ M_\odot$, $p_2 = 3 \times 10^3$ Myr$/M_\odot$). The virial radius r_v of a galaxy with $M = 5 \times 10^{10}\ M_\odot$ at $z = 0$ equals $\sim$218 kpc.

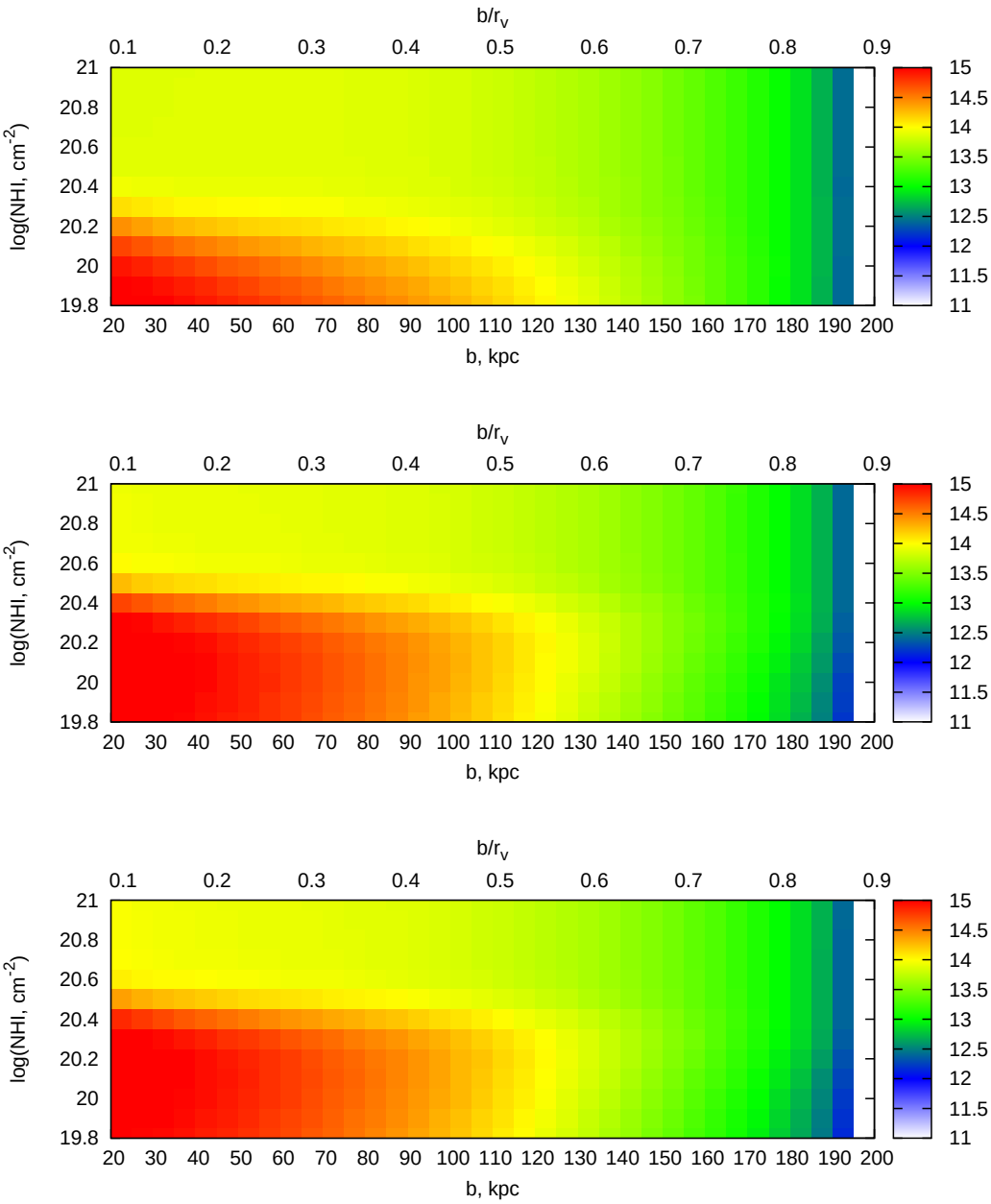
b/r_v
0.1 0.2 0.3 0.4 0.5 0.6 0.7 0.8 0.9
log(NHI, cm^-2)
21 20.8 20.6 20.4 20.2 20 19.8
15 14.5 14 13.5 13 12.5 12 11.5 11
20 30 40 50 60 70 80 90 100 110 120 130 140 150 160 170 180 190 200
b, kpc
b/r_v
0.1 0.2 0.3 0.4 0.5 0.6 0.7 0.8 0.9
log(NHI, cm^-2)
21 20.8 20.6 20.4 20.2 20 19.8
15 14.5 14 13.5 13 12.5 12 11.5 11
20 30 40 50 60 70 80 90 100 110 120 130 140 150 160 170 180 190 200
b, kpc
b/r_v
0.1 0.2 0.3 0.4 0.5 0.6 0.7 0.8 0.9
log(NHI, cm^-2)
21 20.8 20.6 20.4 20.2 20 19.8
15 14.5 14 13.5 13 12.5 12 11.5 11
20 30 40 50 60 70 80 90 100 110 120 130 140 150 160 170 180 190 200
b, kpc

Acknowledgments. E.V. is supported by the Russian Scientific Foundation (grant 14-50-00043). M.R. and Y.S. are supported by the RFBR (grants 15-02-08293, 15-52-45114).

References

1. *J. Tumlinson, C. Thom, J.K. Werk et al.*, Science, **334**, 948, 2011.
2. *R. Bordoloi, J. Tumlinson, J.K. Werk et al.*, Astrophys. J., **796**, 136, 2014.
3. *E.O. Vasiliev, M.V. Ryabova, Yu.A. Shchekinov*, Mon. Not. Roy. Astron. Soc., **446**, 3078, 2015.
4. *G.J. Ferland, K.T. Korista, D.A. Verner et al.*, Publ. Astron. Soc. Pacif., **110**, 761, 1998.
5. *M. Fioc, B. Rocca-Volmerange*, Astron. Astrophys., **326**, 950, 1997.
6. *M. Gilfanov, H.-J. Grimm, R. Sunyaev*, Mon. Not. Roy. Astron. Soc., **347**, L57, 2004.
7. *F. Haardt, P. Madau*, in Clusters of Galaxies and High Redshift Universe Observed in X-rays. Eds. D.M. Neumann, J.T.V. Tran. Rencon. Moriond, 2001.
8. *R. Feldmann, D. Hooper, N.Y. Gnedin*, Astrophys. J., **763**, 21, 2013.
9. *D. Schiminovich, T.K. Wyder, D.C. Martin et. al.*, Astrophys. J. Suppl., **173**, 315, 2007.

* The color figures are available online in the Proceedings at *http://www.astro.spbu.ru/sobolev100/*.